Association of COVID-19 inflammation with activation of the C5a–C5aR1 axis

Julien Carvelli, Olivier Demaria, Frédéric Vély, Luciana Batista, Nassima Chouaki Benmansour, Joanna Fares, Sabrina Carpentier, Marie-Laure Thibult, Ariane Morel, Romain Remark, et al.

▶ **To cite this version:**

Julien Carvelli, Olivier Demaria, Frédéric Vély, Luciana Batista, Nassima Chouaki Benmansour, et al.. Association of COVID-19 inflammation with activation of the C5a–C5aR1 axis. 2024. hal-04831690

HAL Id: hal-04831690

https://amu.hal.science/hal-04831690v1

Preprint submitted on 11 Dec 2024

HAL is a multi-disciplinary open access archive for the deposit and dissemination of scientific research documents, whether they are published or not. The documents may come from teaching and research institutions in France or abroad, or from public or private research centers.

L'archive ouverte pluridisciplinaire **HAL**, est destinée au dépôt et à la diffusion de documents scientifiques de niveau recherche, publiés ou non, émanant des établissements d'enseignement et de recherche français ou étrangers, des laboratoires publics ou privés.

Distributed under a Creative Commons Attribution 4.0 International License

Research Square

Preprints are preliminary reports that have not undergone peer review.
They should not be considered conclusive, used to inform clinical practice,
or referenced by the media as validated information.

Identification of immune checkpoints in COVID-19

Julien Carvelli
Assistance Publique des Hôpitaux de Marseille, Hôpital de la Timone, Réanimation des Urgences, France
Olivier Demaria
Innate Pharma, Marseille, France
Frédéric Vély
Aix Marseille Univ, CNRS, INSERM, CIML, Marseille, France
Luciana Batista
Innate Pharma, Marseille, France
Nassima Chouaki Benmansour
Hôpital d'Instruction des Armées Laveran, Marseille, France
Joanna Fares
Innate Pharma, Marseille, France
Sabrina Carpentier
Innate Pharma, Marseille, France
Marie-Laure Thibult
Innate Pharma, Marseille, France
Ariane Morel
Innate Pharma, Marseille, France
Pascale André
Innate Pharma, Marseille, France
Agnès Represa
Innate Pharma, Marseille, France
Christelle Piperoglou
Aix Marseille Univ, CNRS, INSERM, CIML, Marseille, France
the Explore COVID-19 IPH group
Innate Pharma, Marseille, France
the Explore COVID-19 Medical group
Pierre Yves Cordier
Hôpital d'Instruction des Armées Laveran, Marseille, France
Erwan Le Dault
Hôpital d'Instruction des Armées Laveran, Marseille, France
Christophe Guervilly

Assistance Publique des Hôpitaux de Marseille, Hôpital Nord, Service de Pathologie Infectieuse et Tropicale, France

Pierre Simeone

Assistance Publique des Hôpitaux de Marseille, Hôpital de la Timone, Réanimation des Urgences, France

Marc Gainnier

Assistance Publique des Hôpitaux de Marseille, Hôpital de la Timone, Réanimation des Urgences, France

Yannis Morel

Innate Pharma, Marseille, France

Mikael Ebbo

Assistance Publique des Hôpitaux de Marseille, Hôpital de la Timone, Internal Medicine, France

Nicolas Schleinitz

Assistance Publique des Hôpitaux de Marseille, Hôpital de la Timone, Internal Medicine, France

Eric Vivier (vivier@ciml.univ-mrs.fr)

Innate Pharma, Marseille, France

Research Article

Keywords: COVID-19, immune responses, immune cell phenotyping, soluble factors present in the blood, broncho-alveolar lavage fluid

Posted Date: May 7th, 2020

DOI: https://doi.org/10.21203/rs.3.rs-27340/v1

License: This work is licensed under a Creative Commons Attribution 4.0 International License. Read Full License

---

Version of Record: A version of this preprint was published on July 29th, 2020. See the published version at https://doi.org/10.1038/s41586-020-2600-6.

Abstract

Coronavirus disease 2019 (COVID-19) is a new pandemic acute respiratory disease caused by infection with severe acute respiratory syndrome coronavirus 2 (SARS-CoV-2)[1-3]. We provide here a longitudinal analysis of immune responses, including immune cell phenotyping and assessments of the soluble factors present in the blood and broncho-alveolar lavage fluid (BALF) of patients at various stages of COVID-19 severity: paucisymptomatic, pneumonia and acute respiratory distress syndrome (ARDS). While we confirm a lymphopenia associated with COVID-19 severity[4-7], we report an increase in expression of the NKG2A and PD-1 inhibitory receptors on T and natural killer (NK) cells, as well as an increase in CD39 expression on NK cells, suggesting that therapeutic blocking antibodies targeting these molecules already used for cancer immunotherapy[8] could be repurposed as first line of defense to promote SARS-CoV-2 clearance. In addition, the C5a anaphylatoxin and its receptor C5aR1 (CD88) play a key role in the initiation and maintenance of inflammatory responses, by recruiting neutrophils and monocytes to the lungs[9,10]. We report an increase in soluble C5a levels proportional to COVID-19 severity and high levels of C5aR1 expression in blood and BALF myeloid cells, indicating a potential role of the C5a-C5aR1 axis in the pathophysiology of ARDS. Avdoralimab is a clinical-stage anti-C5aR1 therapeutic monoclonal antibody (mAb) that prevents C5a-mediated myeloid cell recruitment and activation. We propose the use of this antibody to limit myeloid cell infiltration in the lung and to prevent the excessive lung inflammation associated with ARDS in COVID-19 patients.

Background

Most COVID-19 patients present only a few mild symptoms, but about 15% of patients progress to severe pneumonia, and about 5% develop ARDS, for which effective therapeutic strategies are urgently required[1-3]. The immune system plays a dual role in COVID-19, contributing to both virus elimination and ARDS development[11]. A detailed characterization of the immune responses occurring during disease progression from mild to severe forms is thus crucial to an understanding of the ways in which we could manipulate immunity to propose new therapies. In particular, given the urgent need for effective treatments for pneumonia in COVID-19 patients, dissection of the immune responses occurring during the course of COVID-19 could lead to the repurposing of approved immunomodulatory drugs and candidate drugs already tested in clinical trials. We thus analyzed the lymphoid and myeloid compartments in a cohort of 82 individuals: 10 healthy controls (HC), 10 paucisymptomatic COVID-19 patients, 34 patients with pneumonia and 28 patients with ARDS due to SARS-CoV-2 (Supplemental Table 1). We focused on molecular pathways that could either stimulate the antiviral immune response at early stages of COVID-19 to promote SARS-CoV-2 clearance, or block the overt inflammation associated with ARDS. Given the key roles of T and NK cells in controlling viral infection[12,13], we focused on PD-1, NKG2A and CD39 for the stimulation of antiviral immunity, as therapeutic monoclonal antibodies blocking the immunosuppressive function of these molecules are available[14-16]. PD-1 and NKG2A are cell surface receptors, and their engagement with their ligands, PD-L1 and HLA-E, respectively, inhibits the function of T and NK cells[15,17]. CD39 is an ectoenzyme that cleaves extracellular ATP and ADP, which can be

released from dead cells upon viral infection, leading to the generation of adenosine, which has strong immunosuppressive effects on T and NK cells[18].

The absolute numbers of peripheral blood NK, B, $CD4^+$ and $CD8^+$ T lymphocytes were reduced in the pneumonia (pneumo) and ARDS groups compare to healthy controls (HC), consistent with previous results[4-7] (Fig. 1a). No difference was observed between the paucisymptomatic group (Pauci) and HC. We investigated the NK cell subsets further, and found that the proportion of mature NK cells, a subset defined on the basis of its expression of the CD16 and CD57 cell surface receptors, was markedly lower in patients with ARDS (Fig. 1b). Knowing their role in viral infection, the loss of mature NK cells may participate in pulmonary complications occurring in the most severe case of COVID-19[19]. We then analyzed the expression of several immune checkpoints. We observed in the blood the presence of a CD39-expressing NK cell population in the pneumonia and ARDS groups of COVID-19 patients that is absent in the HC and paucisymptomatic groups. Moreover, the cell surface density of CD39, which is known to be upregulated by hypoxia[20], was strongly upregulated in this subset compared to its level in normal conditions (Fig. 1c). The upregulation of CD39 on NK cells has been reported in patients with several types of infection and may be associated with disease progression[21-23]. As opposed to NK cells, CD39 expression was not upregulated on the global population of peripheral $CD4^+$ and $CD8^+$ T cells. In cancers, CD39 expression is mainly found on tumor-reactive CD8 T cells[24] defining T-cell exhaustion[25] and on T regulatory cells[26]. PD-1 was upregulated on NK, $CD4^+$ and $CD8^+$ T lymphocytes in COVID-19 patients, and several ARDS COVID-19 patients had a particularly large subset of NK cells expressing PD-1. The expression of PD-1 on NK cells has been described in some human cancers[27], but the frequency of patients with a PD-1^+ NK cell subset of this size in peripheral blood is uncommon. The NKG2A-expressing NK cell subset was smaller in patients with ARDS, although the cell surface density of NKG2A was upregulated in this same group (Fig. 1c). By contrast, the expression of NKG2C, an activating receptor of HLA-E implicated in the control of CMV viral infections[28], remained unmodified in COVID-19 patients (Extended Fig. 1a). The inhibitory or activating receptors for HLA-C, KIR2DL1/S1 expression were also increased on NK cells of ARDS patients and KIR2DL2/L3/S2, remained unmodified (Extended Fig. 1a). Furthermore, the expression of NKG2A on $CD8^+$ T cells was upregulated in the ARDS group (Fig. 1c). Thus, the cytotoxic lymphocytes involved in controlling viral infection display an upregulation of the inhibitory receptor NKG2A that is associated with COVID-19 severity, consistent with recent results[29]. This upregulation of NKG2A on lymphocyte subsets may be induced by pro-inflammatory cytokines and chronic antigenic stimulation[15]. Remarkably, these changes in NKG2A, PD-1 and CD39 expression were also observed in T and NK cells isolated from the BALFs of ARDS COVID-19 patients and even increased as compared to blood cells in most instances (Fig. 1d, e). Interestingly, an upregulation of *KLRC1,* encoding NKG2A, has been reported in SARS-Cov-2-specific CD8 T cells[30]. Together, these results show that the T and NK cells in the blood and BALF of COVID-19 patients display signs of dysfunction, similarly to some extend to those described in cancer. A longitudinal follow-up study based on immune monitoring in pneumonia and ARDS patients showed that the upregulation of CD39, PD-1 and NKG2A expression on NK, $CD8^+$ or $CD4^+$ T cells initially observed in the first sampling remained stable or even

increased during the course of the disease (Extended Fig. 1d). The blockade of CD39, PD-1 or NKG2A has been shown to harness T and NK cell immunity in cancers[15,31], and in several viral infections[32]. Together, these results support the repurposing of blocking therapeutic mAbs targeting CD39, PD-1 or NKG2A to improve T and NK cell immunity at early stages of the disease, to facilitate elimination of the virus.

Disease severity was also associated with peripheral blood neutrophilia (Fig. 2a). No major changes were observed in the total peripheral blood monocyte population (Fig. 2a). However, the proportion of conventional $CD14^{+}CD16^{-}$ monocytes increased, whereas the proportion of inflammatory $CD14^{-}CD16^{+}$ monocytes decreased in peripheral blood (Fig. 2b), consistent with the possibility of inflammatory monocytes leaving the bloodstream and homing to tissues. This hypothesis was supported by transcriptomic analyses of lung tissues from symptomatic COVID-19 patients, which revealed not only an increase in monocytes and macrophages in the peripheral blood (Extended Fig. 1b), but also an increase in macrophage and monocyte numbers in inflamed lungs (Extended Fig. 1c).

We then analyzed the levels of inflammatory cytokines in the peripheral blood of our cohorts of COVID-19 patients. Consistent with the findings of other studies, we found that the levels of pro-inflammatory cytokines and chemokines, including IL-6, CCL4, CCL2 and CXCL9, were significantly higher in the group of patients with the most severe disease (ARDS) than in the group of paucisymptomatic patients (Fig. 2c). Given the crucial role of myeloid cells in COVID-19 ARDS[30,33], we decided to focus on the complement factor C5a, which mediates strong chemoattraction and activation of myeloid cells[9,10]. The complement system is an important component of immunity that plays a key role in pathogen sensing and clearance[9,10]. The complement cascade implicates several components including cell surface receptors and soluble regulators. In the final phase of the response, the membrane attack complex (MAC), and the potent chemoattractants and inflammatory mediators C3a and C5a are generated. The MAC forms transmembrane channels on the surface of pathogen cells causing disruption of the cell membrane leading to cell death. The C3a and C5a proteins regulate inflammation by binding to their receptors, C3aR and C5aR1[34]. Exaggerated complement activation contributes to the pathogenesis of many inflammatory and immune diseases. C3a and C5a play well-documented roles specifically in lung inflammation and injury. Many studies of the lung epithelium have reported depositions of complement components and suggest that the systemic activation of complement leads, via the potent activity of C5a, to neutrophil recruitment, activation, and adhesion to the pulmonary endothelium, resulting in cell damage and necrosis of the vasculature, and subsequent acute lung injury (ALI). The local activation of complement in the alveoli can cause neutrophil-dependent ALI, resulting in a cytokine/chemokine storm, in which immune cells and nonimmune cells release large amounts of pro-inflammatory cytokines that damage host tissues. This leads to intense ALI and ARDS, which may be fatal[35]. Interestingly, C5a was increased in few patients in the paucisymptomatic group and was significantly higher than those in HC in both groups displaying lung damage: the pneumonia and ARDS groups (Fig. 3a). The upregulation of C5a in patient with the mildest symptoms suggests a role for this anaphylatoxin in the initiation of the cytokine storm occurring in patients progressing to ARDS. An early role of C5a in the initiation of septic events is well-documented and has been shown to be correlated with a strong upregulation of its receptor,

C5aR1 (CD88), in various organs[36-38]. The strong expression of C5aR1 on circulating neutrophils and monocytes in healthy individuals is maintained at all stages of COVID-19 disease progression (Fig. 3b). High levels of C5a in COVID-19 patients have recently been reported to be a consequence of overt activation of the complement cascade by the SARS-COV-2 N-protein[39]. High C5a levels have also been described in various preclinical models of acute lung disease due to highly pathogenic viruses, such as SARS-Cov-1, H1N1, H5N1 and H7N9[40]. High levels of C5a were found in the upper respiratory tract and serum samples from patients infected with H1N1 virus[41]. By contrast, BALF from patients who had recovered from ARDS was found to have significantly lower levels of C5a-dependent chemotactic activity[35,40,42]. In a mouse model of MERS-CoV infection, C5a concentrations were increased in serum samples and in lung tissues[43]. Inhibition of the C5aR1 receptor attenuated lung and spleen tissue damage and reduced inflammatory responses. Importantly, anti-C5aR1 antibody treatment decreased viral replication in lung tissue[43]. In a green monkey model of H7N1 infection, treatment with an anti-C5a antibody significantly decreased the levels of IL-6, IFN-g, TNFa and IL-1b and the neutrophil infiltration into the lungs. Overall, C5a inhibition markedly decreased the ALI and systemic inflammation induced by viral infection[44]. Consistent with these data, C5a increased the production of IL-6, CCL2, CCL4 and TNFa pro-inflammatory cytokines induced by LPS on purified blood monocytes isolated from the various groups of COVID-19 patients and control individuals (Fig. 3c). Importantly, neutrophils and monocytes from the BALF of ARDS patients expressed C5aR1, consistent with high levels of C5a in symptomatic COVID-19 patients that may lead to the chemo-attraction and activation of myeloid cells in the lung and contributing to the overt release of proinflammatory cytokines (Fig. 3d, 3e). The high level of complement pathway activity, and of C5a in particular, was confirmed by transcriptomic analysis on the peripheral blood and BALF of COVID-19 patients (Extended Fig. 3a). Longitudinal immune-monitoring follow-up of patients with pneumonia and ARDS showed that C5a and C5aR1 molecules remained stable or may even increase during the course of the disease (Extended Fig. 3b,c), suggesting that patients might benefit from the blockade of this pro-inflammatory pathway throughout the entire course of COVID-19.

Avdoralimab is a fully human Fc silent mAb against C5aR1 that prevents its binding to C5a. *In vitro*, avdoralimab blocked C5a-induced neutrophil activation, as assessed by evaluating the induction of CD11b cell surface expression (Fig. 4a). Similarly, avdoralimab blocked the neutrophil activation induced by very high concentrations of C5a (Fig. 4b), and its half maximal inhibitory concentration (IC_{50}) in healthy individuals was found to be about 0.3 mg/ml (Fig. 4c). Avdoralimab also effectively inhibited the C5a-induced migration of neutrophils *in vitro* (Fig. 4d). Finally, avdoralimab inhibited the C5a-induced increase in IL-6 and TNFa secretion induced *in vitro* in monocytes purified from paucisymptomatic, pneumonia and ARDS COVID-19 patients, and healthy control individuals (Fig. 4e). In these experiments, monocytes were stimulated with R848, which activates the TLR7/TLR8 MyD88-dependent signaling pathway[45], mimicking the single-stranded RNA of SARS-Cov-2. Avdoralimab is, thus, highly suitable for blocking the C5a-C5aR1 axis, which is active during COVID-19. The high levels of C5a observed in COVID-19 do not appear to be a passenger phenomenon, as two COVID-19 patients recovered from ARDS following treatment with an anti-C5a blocking mAb[39]. There are several advantages to blocking C5aR1

rather than other components of the complement cascade. First, blocking C5aR1 leaves C5b intact and preserves the MAC, which plays a key role in controlling several infections[9 10]. Second, C5aR1 blockade has the advantage over C5a blockade of having no effect on the second C5a receptor, C5L2. The function of C5L2 remains elusive, but it has been suggested that it can act as a decoy receptor, with anti-inflammatory roles[46]. Finally, there is a pharmacological advantage to a terminal complement blockade, as blocking the end product of the cascade, like C5a, is more pharmacologically efficient than blocking upstream components at a single checkpoint. This approach is consistent with the downstream blockade rationale, and the most downstream targetable element is C5aR1, because the inhibition of MAC raises serious safety concerns as severe COVID-19 patients often develop comorbid conditions, such as bacterial infections, for which the MAC is required.

The data presented here support the launching of randomized studies of therapeutic mAbs, alone or in combination with antiviral drugs, to assess the efficacy of their repurposing for the treatment of patients with COVID-19. Anti-PD-(L)1, anti-NKG2A and anti-CD39 mAbs could be tested as a means of boosting T and NK cell antiviral immunity in patients with pneumonia at early stages of SARS-CoV-2 infection, and anti-C5aR1 mAbs could be tested as a mean of preventing or halting the inflammatory mechanisms underlying progression to ARDS in patients at early or late stages of infection. In addition to pneumonia and ARDS, there are data to suggest a role of C5a in other COVID-19-related symptoms, including heart, kidney or endothelial cell dysfunction[47-49], providing further support for the testing of avdoralimab in COVID-19 patients.

Methods

Reagent table

Reagent	Reference	Provider
DPBS (1X)	14190-094	Gibco
RPMI medium 1640 (1X)	31870-025	Gibco
Sodium pyruvate 100 mM (100X)	11360-039	Gibco
L-glutamine 200 mM (100X)	25030-024	Gibco
Minimum essential medium non-essential amino acids solution	11140-035	Gibco
Trypan blue stain (0.4%)	15250-061	Gibco
Ficoll-Paque PLUS	17-1440-03	GE Healthcare
Fetal bovine serum	F7524	Sigma
Dimethyl sulfoxide	D2650-100ML	Sigma
CD14 Microbeads, human	130-050-201	Miltenyi
EasySep direct human neutrophil isolation kit	19666	Stemcell
Bovine serum albumin	A9418-100G	Sigma
UltraPure 0.5 M EDTA, pH 8.0	15575-038	Invitrogen
LPS (LPS EK ultrapure)	tlrl-peklps	Invivogen
R848	tlrl-r848	Invivogen
C5a desArg	N/A	IPH
C5a	2037-C5-025	R&D Systems
avdoralimab	N/A	IPH
Isotypic control (Fc silent hIgG1)	N/A	IPH
CD57-FITC clone NK-1	555619	BD
CD33- PECF594 clone WM53	562492	BD
CD19-PECy7 clone SJ25C1	557835	BD

CD279-BV421 clone EH12.2H7	329920	BioLegend
CD15-BV510 clone W6D3	563141	BD
CD45-BV711 clone HI30	564357	BD
CD56-BV786 clone NCAM16.2	564058	BD
CD16-BUV395 clone 3G8	563785	BD
CD3-BUV496 clone UCHT1	564809/612940	BD
CD14-BUV737 clone M5E2	564444/612763	BD
HLA-DR-AF700 clone L243	307626	BioLegend
LIVE DEAD NEAR IR	L34976	ThermoFisher
Mouse serum	015-000-120	Jackson ImmunoResearch
CD88 C5aR PE clone S5/1	344304	BioLegend
NKG2C PE clone EH12.2H7	329920	BioLegend
NKG2A APC clone REA110	130-113-563	Miltenyi
CD39 APC clone A1	328210	BioLegend
NKG2C PE clone 134591	FAB138P-100	R&D Systems
CD158b1/b2,j (KIR2DL2/L3/S2) PE clone GL183	IM2278U	BC
CD158a/h (KIR2DL1/S1) APC clone 11PB6	130-092-685	Miltenyi
CD45 FITC clone HI30	304038	BioLegend
CD3 BUV496 clone UCHT1	564809/612940	BD
CD8 BUV395 clone RPA-T8	563795	BD
CD4 BV711 clone OKT4	317440	BioLegend
anti-CD16 FITC	556616	BD Biosciences
anti-CD11b PE-Cy5	555389	BD Biosciences

U-PLEX kit	N05235A-1	MSD
OptEIATM huC5a ELISA	557965	BD
RPMI 1640	31870-025	Gibco
Ficoll	11778538	Invitrogen
Dextran	31382	Sigma
PBS	14190-094	Gibco
Calcein AM	C3100MP	Invitrogen
fibrinogen	F3879	Sigma
Transwell Fluoroblok 3 µm insert	351151	Corning
BSA	A9418	Sigma
EDTA	15575-038	Ivitrogen,
Sodium azide	71290-100g	Sigma
Optilyse C solution	A11895	Beckman Coulter
CytoFix	554655	BD Bioscience

Study subjects and clinical considerations

Over a period of one month (03-27-2020 to 04-24-2020), 82 subjects were recruited from three hospitals (Timone and Nord University Hospitals and Laveran Military Hospital, Marseille). 28 of these patients were on mechanical ventilation for COVID-19-related-ARDS (P/F ratio < 300) (ARDS group), 34 patients required oxygen support at a rate of less than 5 L/min for COVID-19-related pneumonia (pneumonia group). 10 patients had a paucisymptomatic form of COVID-19 compatible with outpatient care (paucisymptomatic group). COVID-19 was diagnosed on the basis of positive SARS-CoV-2 rt-PCR on nasopharyngeal samples and/or typical CT-scan findings[50]. We also included 10 healthy volunteers (control group), with no fever or symptoms in the days before sampling and

negative for SARS-CoV-2 rt-PCR. Patient characteristics are presented in Supplementary Table 1. Biological samples were first collected within three days of diagnosis and the start of care (T0: < 72 h, early time-point 1). When possible, the next two time-points for sample collection were located between days 5 and 10 (T1: D5 to D10, intermediate time-point 2) and after day 10 (T2: > D10, late time-point 3). Fresh blood samples (EDTA tubes) and BALFs were analyzed immediately after collection. Clinical progression was evaluated between the early and intermediate time points and between the intermediate and late time points. A favorable outcome was defined as weaning from mechanical ventilation (ARDS group) or oxygen support (pneumonia group). Death or multiple organ failure (ARDS group) and admission to the ICU (pneumonia group) were considered unfavorable outcomes. In other cases, patients were considered to be stable.

Ethics approval statement

All the patients (and/or initially their family) provided written informed consent before sampling and for the use of their clinical and biological data. The study protocol was approved on 03-27-2020 by the Committee for the Protection of Persons Ile-de-France III – France (#2020-A00757-32).

SARS Cov2 detection by PCR

SARS-CoV-2 RNA was assessed by real-time reverse transcription-PCR as described previously[51].

PBMC and plasma preparation

Whole blood collected in EDTA tubes was pooled and diluted 1/2 in PBS. PBMCs were isolated by centrifugation on a Ficoll gradient. PBMCs were collected and 10^7 PBMCs per

vial were frozen in freezing medium (90% FCS + 10% DMSO). Plasma was collected from the upper phase of the Ficoll gradient, aliquoted and used for the quantification of soluble factors.

Soluble factor assessment

Human IL-6, CXCL9, CCL2 and CCL4 were analyzed with the U-PLEX kit supplied by MSD (U-PLEX 10-Assay, 96-Well SECTOR Plate (ref: N05235A-1) according to the manufacturer's instructions. The U-PLEX plate was loaded into an MSD instrument to measure the intensity of emitted light, which is proportional to the amount of analyte present in the sample. Circulating C5a-desArg levels were analyzed with The BD OptEIATM huC5a ELISA test. HRP-conjugated secondary Ab was detected by incubation with a peroxidase substrate solution (TMB), and the reaction was stopped by acidification. Plates were read at 450 nm.

Flow cytometry

Blood collected into EDTA tubes was washed in PBS before staining with LiveDead (ThermoFisher) according to the manufacturer's instructions. Cells were incubated with mouse serum to saturate the Fc receptors, and were then incubated in the appropriate antibody cocktail. Red blood cells were lysed in Optilyse C Solution (Beckman Coulter), according to the manufacturer's instructions. Cells were fixed in Cell Fix solution (BD), according to the manufacturer's instructions. Data were acquired in an LSRFortessaX20 flow cytometer. The FCS3.0 files obtained were exported from BD FACSDiva software and imported into FlowJo v.10.5.2 (BD Biosciences). Automated compensation was calculated by FACSDiva software with single-stained compensation beads. This compensation matrix was analyzed in detail in FlowJo, by investigating the N-by-N view feature and the pairwise expression of all proteins stained in this study. Fluorescence minus one (FMO) experiments were run before this study, to facilitate optimization of the compensation matrix. We then

adjusted the compensation matrix where necessary due to over- or under-compensation by the automatic algorithm. After adjustment of the compensation matrix, samples were concatenated and analyzed with the FlowJo UMAP plugin (v2.2). UMAP was run with the default settings (Euclidean distance function, nearest neighbors: 15 and minimum distance: 0.5). UMAP projections were obtained for concatenated cells from healthy donors (n=10), paucisymptomatic (n=8), pneumonia (n=13) and ARDS (n=10) patients. The UMAP parameters were selected according to the experimental question addressed and are specified in the accompanying text and figure legends.

Immune cell counts

Absolute counts per µL of blood were determined with BD TBNK Trucount™ Tubes. Absolute counts for a particular cell population (A) were obtained by dividing the number of positive cell events (X) by the number of bead events (Y), and then multiplying by the BD Trucount bead concentration (N/V, where N = number of beads per test* and V = test volume). A = X/Y × N/V. The number of positive counts for each immune population was established with the following gating strategies: NK cells, $CD45^+$ $CD3^-CD16^+CD56^+$; B cells, $CD45^+CD3^-CD19^+$; CD4 T cells, $CD45^+CD3^+CD4^+$; CD8T cells $CD45^+CD3^+CD8^+$; neutrophils, $CD45^+SSC^{high}$; monocytes, $CD45^+SSC^{int}$.

Neutrophil migration

Neutrophils were isolated from fresh blood by a first step of sedimentation in 6% dextran to sort plasma and leukocytes followed by a gradient of ficoll. The pellet, containing neutrophils, was recovered, and the red blood cells were lysed by incubation in 0.2% NaCl . Osmotic balance was restored by adding an equal volume of 1.6% NaCl. Isolated neutrophils were loaded with 10 µM Calcein AM. Cell density was adjusted before the addition of avdoralimab or its isotype control at a final concentration of 10 µg/mL.

Neutrophils were dispensed into the top chamber of a fibrinogen- and BSA-coated Transwell Fluoroblok 3 µm insert. The lower chamber was filled with RPMI 1640 with or without 3 nM C5a (R&D Systems,) and the same antibody was added to the top chamber (avdoralimab, isotype control or PBS). After 30 minutes of incubation at +37 ± 1°C under an atmosphere containing 5 ± 1% CO_2, images of the lower face of the inserts were acquired on a Biotek Cytation 5 plate-reading microscope, and analyzed with Halo software (Indica labs), using the CytoNuclear FL module to count the cells that had crossed the membrane. The % migration was calculated for avdoralimab and its isotype control, by subtracting the spontaneous migration observed without C5a, and dividing by the migration observed in the absence of antibodies: 100 x [(Ab with C5a) - (no Ab no C5a)] / [(no Ab with C5a) - (no Ab no C5a)].

Neutrophil activation

Various concentrations of avdoralimab were added to the blood samples in culture-treated 96-well U-bottom plates, and incubated for 20 min at 37°C under an atmosphere containing 5% CO_2. Then, 18 nM of human recombinant C5a (R&D Systems) were added to the samples. Plates were incubated for 20 minutes at 37°C under an atmosphere containing 5% CO_2. Samples were then stained for flow cytometry analysis with anti-CD16 FITC and anti-CD11b PE-Cy5 antibodies. Erythrocytes were lysed with Optilyse C solution (Beckman Coulter, A11895), according to the manufacturer’s protocol, and resuspended in CytoFix (BD Bioscience 554655) for fixation. Cells were then analyzed on a FACS Canto II flow cytometer (BD Biosciences) with FACS Diva software.

Transcriptomic analysis

Transcriptomics analyses were performed on data previously described[52]. The RNASeq data for two BALF samples from patients (each in duplicate), three PBMC samples from

healthy controls and three PBMC samples from patients were downloaded from the National Genomics Data Center (https://bigd.big.ac.cn/) under the accession number PRJCA002326. The RNA-seq data for three BALF samples from healthy controls were downloaded from the SRA database under accession numbers: SRR10571724, SRR10571730, and SRR10571732. RNASeq pipeline: The reads were mapped to human genome (hg38) release 96 from Ensembl with STAR[53]. PCR replicates mapping to the human genome were removed with the Picard MarkDuplicates program (Broad Institute 2019, http://broadinstitute.github.io/picard/). Gene expression was calculated with featureCounts in the SubReads package (v1.6.4)[54]. TPM (transcripts per million) values were calculated from the raw counts and log2-transformed. The depth of sequencing of the patients' BALF samples was low (< 1 M).

Batch effect correction: we corrected for the batch effect between the datasets for BALF samples from healthy donors and those from patients and PBMC samples with Combat[55], using the model: ~ Batch + Status (Patient or Healthy) + Sample Type (PMBC or BALF).

Immune cell score calculation: we calculated immune cell scores as the sum of the expression, in log2-tpm, of representative aggregate genes called metagenes. The NK metagene was defined as a 13-gene signature[56]: CD160, CD244, CHST12, CST7, GNLY, IL18RAP, IL2RB, KLRC1, KLRC3, KLRD1, KLRF1, PRF1, XCL2, to which we added NCR1. The other metagenes were defined with the signature matrix file LM22 obtained with CIBERSORT[57] by selecting the genes with the highest weights for the population of interest. The specificity of each list was then validated with an immune cell compendium[58]. The CD8T metagene was defined as: CD3, CD3D, CD8A, CD8B, KLRC1, KLRK1, GZMH and CCL5. The CD4T metagene was: CD3E, CD3D, CD4, CTLA4 and ICOS. The monocyte metagene was: CD14, FCN1 and AIF1, and the macrophage metagene was: MMP9, PLA2G7, CYP27A1, ADAMDEC1, CD68 and CD163.

Complement pathway score calculation: complement pathway scores were defined as the sum of the expression, in log2-tpm, of representative metagenes. Complement pathway

metagenes were defined as described in a previous study[59]. The metagene used for the classical pathway was: C1QA, C1QB, C1QC, C1R and C1S. The metagene used for the lectin-pathway was: FCN1, FCN2, FCN3, MASP1 and MASP2. For the alternative pathway, the metagene used was: C3, CFB, CFD and CFP.

Data analysis and statistics

All statistics analyses were performed with R (version 3.6.1). Packages ggpubr (version 0.2.5) and lmerTest (version 3.1.2) were used for statistical tests. Package gtsummary (version 1.3.0) for used for clinical tables. Package sva (version 3.32.1) was used to correct the batch effect of RNAseq. Package fmsb (version 0.6.3) was used to draw radar charts. For the comparison of groups at timepoint T0, p-values were obtained for two-sided Wilcoxon rank-sum tests. For longitudinal analysis in the pneumonia group, p-values for comparisons of T1 and T0 were obtained in two-sided Wilcoxon signed-rank tests. No statistic tests were performed for T2 in this group. For the ARDS group, a mixed model was computed with timepoint as a fixed effect (categorical variable) and patient as a random effect. Confidence intervals and p-values were obtained based on the t-distribution, with degrees of freedom according to the Kenward-Roger method and the normality of residuals was verified. Plots were drawn using GraphPad Prism version 8.1.1. Boxplots represent the median and 25th to 75th percentiles and the whiskers denote lowest and highest values.

Declarations

Acknowledgments: We thank Sophie Ugolini (Centre d'Immunologie de Marseille-Luminy) for helpful advice, all the healthcare workers involved in the analysis, diagnosis and treatment of patients at AP-HM and Hôpital Laveran, especially Luc Lyonnet, Elise Kaspi, Eric Garnotel, Corinne Surcouf, Francois Xavier Le Flem (Bataillon des Marins Pompiers Marseille). We thank all our patients, supporters and families for their confidence in our work. The E.V. laboratory at CIML and Assistance-Publique des Hôpitaux de Marseille is supported by funding from the European Research Council (ERC) under the European Union's Horizon 2020 research and innovation program (TILC, grant agreement No. 694502 and MInfla-TILC, grant agreement No. 875102 - MInfla-Tilc), the *Agence Nationale de la Recherche* including the PIONEER Project (ANR-17-RHUS-0007), MSDAvenir, Innate Pharma and institutional grants to the CIML (INSERM, CNRS, and Aix-Marseille University) and to Marseille Immunopole.

Explore COVID-19 IPH group: William Baron, Nourhène Belaid, Clarisse Caillet, Barbara Carrette, Florent Carrette, Rachel Courtois, Aurore Fenis, Marilyn Giordano, Mathilde Girard-Madoux, Marc Giraudon-Paoli, Nicolas Gourdin, Gwendoline Grondin, Franceline Guillot, Solène Jaubert, Julie Lopez, Mélanie Le Van, Naouel Lovera, Marine Mansuy, Elodie Bonnet, Audrey Sansaloni, Annick Reboul, Emmanuel Mitry, Camille Nekkar-Constant, Valentine Péri, Paul Ricaut, Jean-Baptiste Vallier, Marie Vétizou, Robert Zerbib

Explore COVID-19 Medical group: Jean-Marie Forel, Laurent Papazian, Lionel Velly, Baptiste André, Antoine Briantais, Benoit Faucher, Estelle Jean, Julie Seguier, Veronique Veit, Jean-Robert Harlé (AP-HM), Axelle Clerc, Emmanuel Delmond, Pierre-Olivier Vidal, Hélène Savini (Hôpital d'Instruction des Armées Laveran)

Author contributions: J.C, F.V. and E.V initiated and designed the research. O.D and E.V. wrote the manuscript with the help of other coauthors. O.D., L.B., J.F. S.C., M-L.T., A.M., P.A., C.P., L.L., W.B., N.B., C.C., B.C., F.C., R.C., A.F., M.G., M.G-M., M.G-P., N.G., G.G., F.G., S.J., J.L., M. L-V., N.L., M.M., C.N-C., V.P., A.R., P.R., J-B.V., M.V., E.B., A.S., A.R., Y. M., E. M., R. Z. performed the experiments and analyzed and/or interpreted results. J-M.F, L.P., L.V., B.A., A.B., B.F., E.J, J.S., V.V., J-R.H., A.C., E.D., P-O.V., H.S., J.C., N.C.B, M. G., J-M.F., L.P., M.E. and N.S. were in charge of patient care and contributed to the discussion of the results.

Competing interests: O.D., L.B., J.F. S.C., M-L.T., A.M., P.A., E.V. W.B., N.B., C.C., B.C., F.C., R.C., A.F., M.G., M.G-M., M.G-P., N.G., G.G., F.G., S.J., J.L., M. L-V., N.L., M.M., C.N-C., V.P., A.R., P.R., J-B.V., M.V., Y. M., E. M., R. Z. are employees of Innate Pharma.

None of the other authors has any competing financial interests to declare.

References

1 Zhu, N. *et al.* A Novel Coronavirus from Patients with Pneumonia in China, 2019. *The New England journal of medicine* **382**, 727-733, doi:10.1056/NEJMoa2001017 (2020).

2 Gorbalenya, A. E. *et al.* The species Severe acute respiratory syndrome-related coronavirus: classifying 2019-nCoV and naming it SARS-CoV-2. *Nature microbiology* **5**, 536-544, doi:10.1038/s41564-020-0695-z (2020).

3 Wolfel, R. *et al.* Virological assessment of hospitalized patients with COVID-2019. *Nature*, doi:10.1038/s41586-020-2196-x (2020).

4 Thevarajan, I. *et al.* Breadth of concomitant immune responses prior to patient recovery: a case report of non-severe COVID-19. *Nature medicine* **26**, 453-455, doi:10.1038/s41591-020-0819-2 (2020).

5 Hadjadj, J. *et al.* Impaired type I interferon activity and exacerbated inflammatory responses in severe Covid-19 patients. *medRxiv*, 2020.2004.2019.20068015, doi:10.1101/2020.04.19.20068015 (2020).

6 Qin, C. *et al.* Dysregulation of immune response in patients with COVID-19 in Wuhan, China. *Clinical infectious diseases : an official publication of the Infectious Diseases Society of America*, doi:10.1093/cid/ciaa248 (2020).

7 Wang, F. *et al.* Characteristics of peripheral lymphocyte subset alteration in COVID-19 pneumonia. *The Journal of infectious diseases*, doi:10.1093/infdis/jiaa150 (2020).

8 Demaria, O. *et al.* Harnessing innate immunity in cancer therapy. *Nature* **574**, 45-56, doi:10.1038/s41586-019-1593-5 (2019).

9 Mastellos, D. C., Ricklin, D. & Lambris, J. D. Clinical promise of next-generation complement therapeutics. *Nature reviews. Drug discovery* **18**, 707-729, doi:10.1038/s41573-019-0031-6 (2019).

10 Pio, R., Ajona, D., Ortiz-Espinosa, S., Mantovani, A. & Lambris, J. D. Complementing the Cancer-Immunity Cycle. *Frontiers in immunology* **10**, 774, doi:10.3389/fimmu.2019.00774 (2019).

11 Shi, Y. *et al.* COVID-19 infection: the perspectives on immune responses. *Cell death and differentiation* **27**, 1451-1454, doi:10.1038/s41418-020-0530-3 (2020).

12 Hammer, Q., Ruckert, T. & Romagnani, C. Natural killer cell specificity for viral infections. *Nature immunology* **19**, 800-808, doi:10.1038/s41590-018-0163-6 (2018).

13 Schmidt, M. E. & Varga, S. M. The CD8 T Cell Response to Respiratory Virus Infections. *Frontiers in immunology* **9**, 678, doi:10.3389/fimmu.2018.00678 (2018).

14 Xin Yu, J. *et al.* Trends in clinical development for PD-1/PD-L1 inhibitors. *Nature reviews. Drug discovery* **19**, 163-164, doi:10.1038/d41573-019-00182-w (2020).

15 Andre, P. *et al.* Anti-NKG2A mAb Is a Checkpoint Inhibitor that Promotes Anti-tumor Immunity by Unleashing Both T and NK Cells. *Cell* **175**, 1731-1743 e1713, doi:10.1016/j.cell.2018.10.014 (2018).

16 Perrot, I. *et al.* Blocking Antibodies Targeting the CD39/CD73 Immunosuppressive Pathway Unleash Immune Responses in Combination Cancer Therapies. *Cell reports* **27**, 2411-2425 e2419, doi:10.1016/j.celrep.2019.04.091 (2019).

17 Sun, C., Mezzadra, R. & Schumacher, T. N. Regulation and Function of the PD-L1 Checkpoint. *Immunity* **48**, 434-452, doi:10.1016/j.immuni.2018.03.014 (2018).

18 de Andrade Mello, P., Coutinho-Silva, R. & Savio, L. E. B. Multifaceted Effects of Extracellular Adenosine Triphosphate and Adenosine in the Tumor-Host Interaction and Therapeutic Perspectives. *Frontiers in immunology* **8**, 1526, doi:10.3389/fimmu.2017.01526 (2017).

19 Guzman, J. *et al.* Phenotypic analysis of bronchoalveolar lavage lymphocytes from acquired immunodeficiency patients with and without Pneumocystis carinii pneumonia. *Acta cytologica* **36**, 900-904 (1992).

20 Eltzschig, H. K. *et al.* Coordinated adenine nucleotide phosphohydrolysis and nucleoside signaling in posthypoxic endothelium: role of ectonucleotidases and adenosine A2B receptors. *The Journal of experimental medicine* **198**, 783-796, doi:10.1084/jem.20030891 (2003).

21 Dierks, P. *et al.* Brief Report: Increased Frequency of CD39+ CD56bright Natural Killer Cells in HIV-1 Infection Correlates With Immune Activation and Disease Progression. *J Acquir Immune Defic Syndr* **74**, 467-472, doi:10.1097/QAI.0000000000001266 (2017).

22 Seshadri, A. *et al.* Altered monocyte and NK cell phenotypes correlate with posttrauma infection. *The journal of trauma and acute care surgery* **87**, 337-341, doi:10.1097/TA.0000000000002264 (2019).

23 Csoka, B. *et al.* CD39 improves survival in microbial sepsis by attenuating systemic inflammation. *FASEB journal : official publication of the Federation of American Societies for Experimental Biology* **29**, 25-36, doi:10.1096/fj.14-253567 (2015).

24 Duhen, T. *et al.* Co-expression of CD39 and CD103 identifies tumor-reactive CD8 T cells in human solid tumors. *Nature communications* **9**, 2724, doi:10.1038/s41467-018-05072-0 (2018).

25 Canale, F. P. *et al.* CD39 Expression Defines Cell Exhaustion in Tumor-Infiltrating CD8(+) T Cells. *Cancer research* **78**, 115-128, doi:10.1158/0008-5472.CAN-16-2684 (2018).

26 Deaglio, S. *et al.* Adenosine generation catalyzed by CD39 and CD73 expressed on regulatory T cells mediates immune suppression. *The Journal of experimental medicine* **204**, 1257-1265, doi:10.1084/jem.20062512 (2007).

27 Pesce, S. *et al.* PD/1-PD-Ls Checkpoint: Insight on the Potential Role of NK Cells. *Frontiers in immunology* **10**, 1242, doi:10.3389/fimmu.2019.01242 (2019).

28 Guma, M. *et al.* Imprint of human cytomegalovirus infection on the NK cell receptor repertoire. *Blood* **104**, 3664-3671, doi:10.1182/blood-2004-05-2058 (2004).

29 Zheng, M. *et al.* Functional exhaustion of antiviral lymphocytes in COVID-19 patients. *Cellular & molecular immunology*, doi:10.1038/s41423-020-0402-2 (2020).

30 Liao, M. *et al.* The landscape of lung bronchoalveolar immune cells in COVID-19 revealed by single-cell RNA sequencing. *medRxiv*, 2020.2002.2023.20026690, doi:10.1101/2020.02.23.20026690

(2020).

31 Young, A., Mittal, D., Stagg, J. & Smyth, M. J. Targeting cancer-derived adenosine: new therapeutic approaches. *Cancer discovery* **4**, 879-888, doi:10.1158/2159-8290.CD-14-0341 (2014).

32 Lee, J., Ahn, E., Kissick, H. T. & Ahmed, R. Reinvigorating Exhausted T Cells by Blockade of the PD-1 Pathway. *Forum on immunopathological diseases and therapeutics* **6**, 7-17, doi:10.1615/ForumImmunDisTher.2015014188 (2015).

33 Liu, J. *et al.* Neutrophil-to-Lymphocyte Ratio Predicts Severe Illness Patients with 2019 Novel Coronavirus in the Early Stage. *medRxiv*, 2020.2002.2010.20021584, doi:10.1101/2020.02.10.20021584 (2020).

34 Guo, R. F., Riedemann, N. C. & Ward, P. A. Role of C5a-C5aR interaction in sepsis. *Shock* **21**, 1-7, doi:10.1097/01.shk.0000105502.75189.5e (2004).

35 Bosmann, M. & Ward, P. A. Role of C3, C5 and anaphylatoxin receptors in acute lung injury and in sepsis. *Advances in experimental medicine and biology* **946**, 147-159, doi:10.1007/978-1-4614-0106-3_9 (2012).

36 Riedemann, N. C. *et al.* Increased C5a receptor expression in sepsis. *The Journal of clinical investigation* **110**, 101-108, doi:10.1172/JCI15409 (2002).

37 Riedemann, N. C. *et al.* Protective effects of IL-6 blockade in sepsis are linked to reduced C5a receptor expression. *J Immunol* **170**, 503-507, doi:10.4049/jimmunol.170.1.503 (2003).

38 Huber-Lang, M. S. *et al.* Protective effects of anti-C5a peptide antibodies in experimental sepsis. *FASEB journal : official publication of the Federation of American Societies for Experimental Biology* **15**, 568-570, doi:10.1096/fj.00-0653fje (2001).

39 Gao, T. *et al.* Highly pathogenic coronavirus N protein aggravates lung injury by MASP-2-mediated complement over-activation. *medRxiv*, 2020.2003.2029.20041962, doi:10.1101/2020.03.29.20041962 (2020).

40 Wang, R., Xiao, H., Guo, R., Li, Y. & Shen, B. The role of C5a in acute lung injury induced by highly pathogenic viral infections. *Emerging microbes & infections* **4**, e28, doi:10.1038/emi.2015.28 (2015).

41 Bjornson, A. B., Mellencamp, M. A. & Schiff, G. M. Complement is activated in the upper respiratory tract during influenza virus infection. *The American review of respiratory disease* **143**, 1062-1066, doi:10.1164/ajrccm/143.5_Pt_1.1062 (1991).

42 Sun, S. *et al.* Inhibition of complement activation alleviates acute lung injury induced by highly pathogenic avian influenza H5N1 virus infection. *American journal of respiratory cell and molecular biology* **49**, 221-230, doi:10.1165/rcmb.2012-0428OC (2013).

43 Jiang, Y. *et al.* Blockade of the C5a-C5aR axis alleviates lung damage in hDPP4-transgenic mice infected with MERS-CoV. *Emerging microbes & infections* **7**, 77, doi:10.1038/s41426-018-0063-8 (2018).

44 Sun, S. *et al.* Treatment with anti-C5a antibody improves the outcome of H7N9 virus infection in African green monkeys. *Clinical infectious diseases : an official publication of the Infectious Diseases Society of America* **60**, 586-595, doi:10.1093/cid/ciu887 (2015).

45 Hemmi, H. *et al.* Small anti-viral compounds activate immune cells via the TLR7 MyD88-dependent signaling pathway. *Nature immunology* **3**, 196-200, doi:10.1038/ni758 (2002).

46 Gerard, N. P. *et al.* An anti-inflammatory function for the complement anaphylatoxin C5a-binding protein, C5L2. *The Journal of biological chemistry* **280**, 39677-39680, doi:10.1074/jbc.C500287200 (2005).

47 Fattahi, F. & Ward, P. A. Complement and sepsis-induced heart dysfunction. *Molecular immunology* **84**, 57-64, doi:10.1016/j.molimm.2016.11.012 (2017).

48 Tan, S. M. *et al.* Complement C5a Induces Renal Injury in Diabetic Kidney Disease by Disrupting Mitochondrial Metabolic Agility. *Diabetes* **69**, 83-98, doi:10.2337/db19-0043 (2020).

49 Varga, Z. *et al.* Endothelial cell infection and endotheliitis in COVID-19. *Lancet*, doi:10.1016/S0140-6736(20)30937-5 (2020).

50 Ai, T. *et al.* Correlation of Chest CT and RT-PCR Testing in Coronavirus Disease 2019 (COVID-19) in China: A Report of 1014 Cases. *Radiology*, 200642, doi:10.1148/radiol.2020200642 (2020).

51 Amrane, S. *et al.* Rapid viral diagnosis and ambulatory management of suspected COVID-19 cases presenting at the infectious diseases referral hospital in Marseille, France, - January 31st to March 1st, 2020: A respiratory virus snapshot. *Travel medicine and infectious disease*, 101632, doi:10.1016/j.tmaid.2020.101632 (2020).

52 Xiong, Y. *et al.* Transcriptomic characteristics of bronchoalveolar lavage fluid and peripheral blood mononuclear cells in COVID-19 patients. *Emerging microbes & infections* **9**, 761-770, doi:10.1080/22221751.2020.1747363 (2020).

53 Dobin, A. *et al.* STAR: ultrafast universal RNA-seq aligner. *Bioinformatics* **29**, 15-21, doi:10.1093/bioinformatics/bts635 (2013).

54 Liao, Y., Smyth, G. K. & Shi, W. featureCounts: an efficient general purpose program for assigning sequence reads to genomic features. *Bioinformatics* **30**, 923-930, doi:10.1093/bioinformatics/btt656 (2014).

55 Johnson, W. E., Li, C. & Rabinovic, A. Adjusting batch effects in microarray expression data using empirical Bayes methods. *Biostatistics* **8**, 118-127, doi:10.1093/biostatistics/kxj037 (2007).

56 Crinier, A. *et al.* High-Dimensional Single-Cell Analysis Identifies Organ-Specific Signatures and Conserved NK Cell Subsets in Humans and Mice. *Immunity* **49**, 971-986 e975, doi:10.1016/j.immuni.2018.09.009 (2018).

57 Newman, A. M. *et al.* Robust enumeration of cell subsets from tissue expression profiles. *Nature methods* **12**, 453-457, doi:10.1038/nmeth.3337 (2015).

58 Carpentier, S., Romagne, F. & Vivier, E. A comprehensive approach to gene expression profiling in immune cells. *Methods in enzymology* **636**, 1-47, doi:10.1016/bs.mie.2019.07.005 (2020).

59 Roumenina, L. T., Daugan, M. V., Petitprez, F., Sautes-Fridman, C. & Fridman, W. H. Context-dependent roles of complement in cancer. *Nature reviews. Cancer* **19**, 698-715, doi:10.1038/s41568-019-0210-0 (2019).

Table

Characteristic	Overall, N = 72	Paucisymp, N = 10[1]	Pneumonia, N = 34[1]	ARDS, N = 28[1]
Age	61 (50, 68)	43 (31, 61)	60 (50, 70)	63 (55, 68)
Gender				
F	19 (26%)	1 (10%)	12 (35%)	6 (21%)
M	53 (74%)	9 (90%)	22 (65%)	22 (79%)
Medical History				
Diabetes	22 (31%)	1 (10%)	9 (26%)	12 (43%)
Obesity	17 (24%)	1 (10%)	5 (15%)	11 (39%)
Arterial hypertension	24 (33%)	2 (20%)	9 (26%)	13 (46%)
Other cardiovascular disease[2]	13 (18%)	2 (20%)	7 (21%)	4 (14%)
Immunosupression[3]	5 (7.0%)	1 (10%)	3 (9.1%)	1 (3.6%)
CT scan				
Normal	1 (1.4%)	1 (10%)	0 (0%)	0 (0%)
Mild	7 (9.7%)	3 (30%)	4 (12%)	0 (0%)
Moderate	27 (38%)	1 (10%)	20 (59%)	6 (21%)
Severe	28 (39%)	0 (0%)	9 (26%)	19 (68%)
NA	9 (12%)	5 (50%)	1 (2.9%)	3 (11%)
Covid-19 diagnosis				
Positive SARS-CoV-2 RT-PCR	50 (69%)	8 (80%)	20 (59%)	22 (79%)
Days since beginning of symptoms[3]	10.0 (7.0, 14.0)	13.0 (9.5, 15.8)	9.5 (7.0, 13.0)	11.0 (7.0, 13.5)
Oxygen requirement				
0	15 (21%)	9 (90%)	6 (18%)	0 (0%)
<5 L/min	13 (18%)	0 (0%)	13 (38%)	0 (0%)
≥5 L/min	32 (44%)	0 (0%)	4 (12%)	28 (100%)
NA	12 (17%)	1 (10%)	11 (32%)	0 (0%)
Pulmonary involvement				
PaO_2/FiO_2 ratio				
>300	32 (52%)	NA	32 (94%)	0 (0%)
Mild ARDS	5 (8.1%)	NA	2 (5.9%)	3 (11%)
Moderate ARDS	17 (27%)	NA	0 (0%)	17 (61%)
Severe ARDS	8 (13%)	NA	0 (0%)	8 (29%)
SOFA[4]				
≤2	48 (67%)	10 (100%)	34 (100%)	4 (14%)
3-4	6 (8.3%)	0 (0%)	0 (0%)	6 (21%)
5-6	5 (6.9%)	0 (0%)	0 (0%)	5 (18%)
≥7	13 (18%)	0 (0%)	0 (0%)	13 (46%)
Leucocytes (G/L) [5]	7.2 (5.5, 11.0)	5.4 (5.4, 5.4)	6.0 (4.9, 7.4)	9.4 (6.8, 13.8)
Neutrophils (G/L) [5]	6.0 (4.1, 9.6)	4.1 (4.1, 4.1)	4.3 (3.5, 6.2)	7.1 (5.6, 12.5)
Lymphocytes (G/L) [5]	1.04 (0.70, 1.40)	1.37 (0.80, 1.58)	1.21 (0.88, 1.51)	0.69 (0.56, 1.06)
Monocytes (G/L) [5]	0.49 (0.30, 0.73)	0.19 (0.19, 0.19)	0.62 (0.32, 0.69)	0.48 (0.32, 0.79)
Platelets (G/L) [5]	227 (174, 296)	197 (183, 246)	221 (164, 264)	241 (176, 305)
Eosinophils (G/L) [5]	0.04 (0.01, 0.16)	0.06 (0.03, 0.11)	0.02 (0.00, 0.13)	0.10 (0.01, 0.20)

[1] Statistics presented: median (IQR); n (%)

[2] Medical history of heart failure, coronary artery disease, stroke or other atherosclerosis complications

[3] Information missing for 1 patient

[4] SOFA: Sequential Organ Failure Assessment score (Vincent JL et al. Intensive Care Med.1996;22(7):707-10. doi: 10.1007/bf01709751)

[5] G/L: x 10^9 / liter. Information missing for some patients

Healthy Donors (N=10): Age *median (IQR):* 54 (42, 57) Gender *n (%):* F: 2 (20%) M: 8 (80%)

Figures

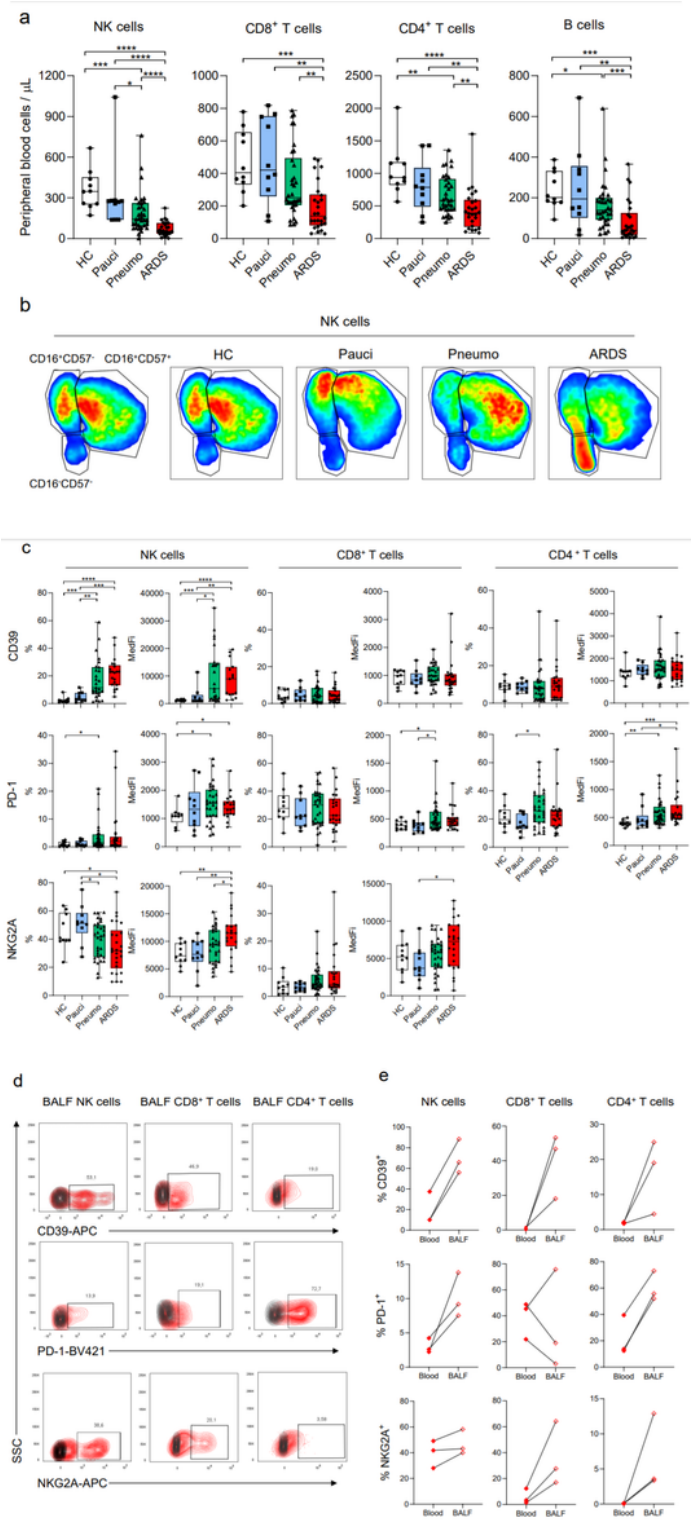

Figure 1

l Covid19 is associated with lymphopenia and modulation of the lymphocyte phenotype. a, Absolute numbers of circulating NK, B, CD4+ and CD8+ T cells per µL of peripheral blood from healthy donors and COVID-19 patients at T0. Each symbol represents a single donor. b, UMAP with color-coding by cell density of concatenated peripheral blood NK cells, with CD56, CD16 and CD57 included in the list of running parameters. Left: the projection of concatenated peripheral NK cells from all samples identifies 3 NK clusters: CD16-CD57-, CD16+CD57- and CD16+CD57+. Right: projections of concatenated peripheral blood NK cells from healthy donors and COVID-19 patients. Red corresponds to the highest cell density. c, Percentages of CD39+, PD-1+ and NKG2A+ NK cells, CD8+ T and CD4+ T cells; MedFi of CD39, PD-1 and NKG2A on CD39+, PD-1+ and NKG2A+ NK, CD8+ T and CD4+ T cells, respectively; in peripheral blood from healthy donors and COVID-19 patients at T0. Each symbol represents a single donor. d, FACS dot plots of CD39, PD-1 and NKG2A expression (red) vs fmo (black) on NK cells, CD8+ T cells and CD4+ T cells from BALF of ARDS patients. Pictures are representative of 3 donors. e, Percentages of CD39+, PD-1+ and NKG2A+ NK cells, CD8+ T cells and CD4+ T cells in blood (full diamond) and BALF (empty diamond) from the same ARDS patients. a-c, HC (healthy controls, white, n=10), Pauci (paucisymptomatic, blue, n=9 to 10), Pneumo (pneumonia, green, n=27 to 34) and ARDS (red, n=21 to 26). p-values were computed using Wilcoxon tests: *p<0.05; **p<0.01; ***p<0.001;****p<0.0001.

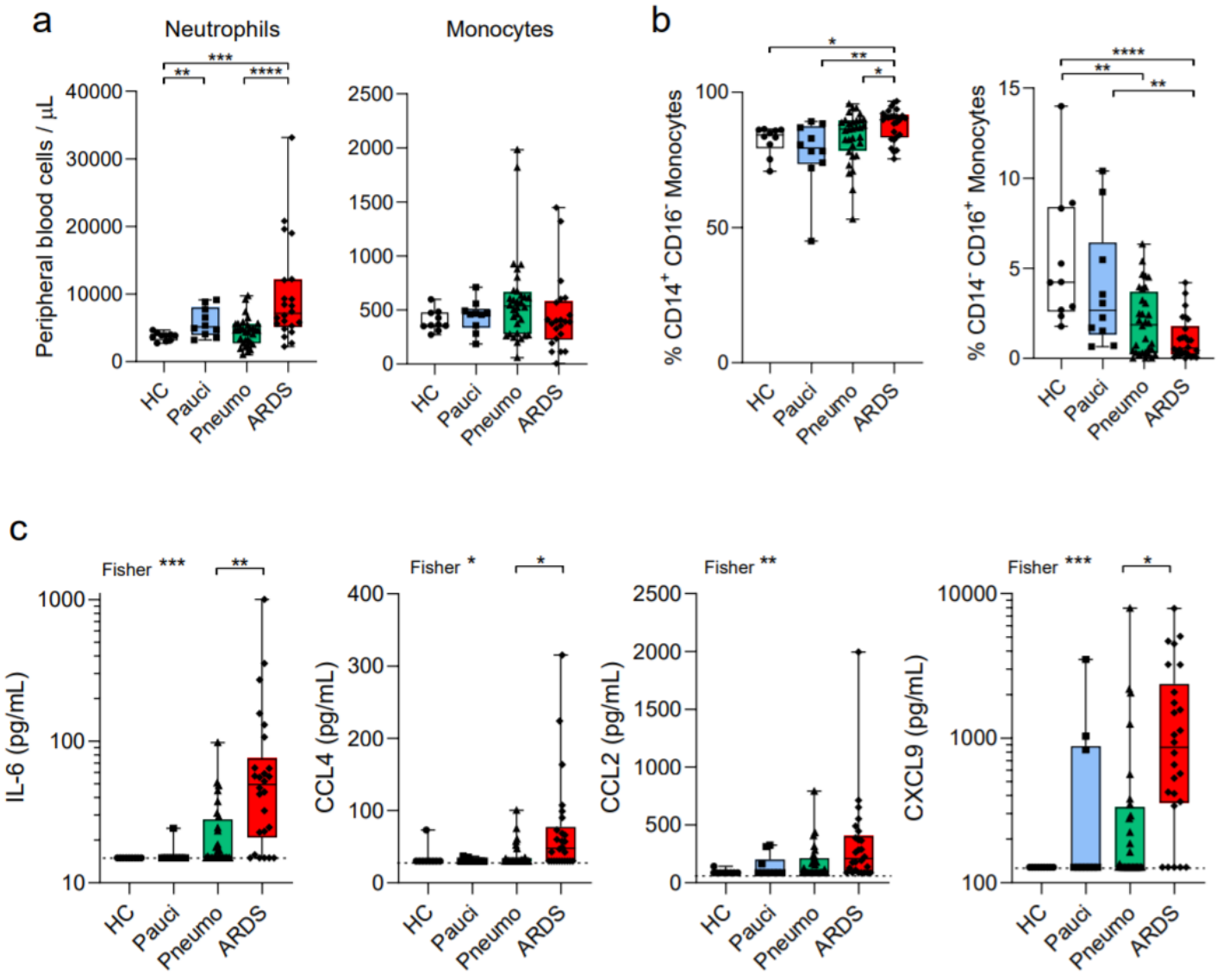

Figure 2

l COVID-19 progression is associated with a modulation of the myeloid cell compartment and a cytokine storm. a, Absolute numbers of circulating neutrophils and monocytes per µL of peripheral blood from healthy donors and COVID-19 patients at T0. Each symbol represents a single donor. b, Percentages of CD14+CD16- conventional monocytes and CD14-CD16+ inflammatory monocytes in the peripheral blood of healthy donors and COVID-19 patients at T0. Each symbol represents a single donor. c, Concentration of IL-6, CCL4, CCL2 and CXCL9 in plasma from healthy donors and COVID-19 patients at T0. Each symbol represents a single donor. Dashed line represents the limit of quantification (LOQ) a-c, HC (healthy controls, white, n=9), pauci (paucisymptomatic, blue, n=6 to 10), pneumo (pneumonia, green, n=27 to 30) and ARDS (red, n=21 to 25). The p-values were obtained using Wilcoxon tests for a-b. For c, first a global comparison was performed by classifying all values in 2 categories: above LOQ or not (p-values from a

Fisher Exact test shows that there is an increase of values above LOQ with increasing severity) and second, a comparison between Pneumonia and ARDS only for the values above the LOQ (p-values from a Wilcoxon test) *p<0.05; **p<0.01; ***p<0.001;****p<0.0001.

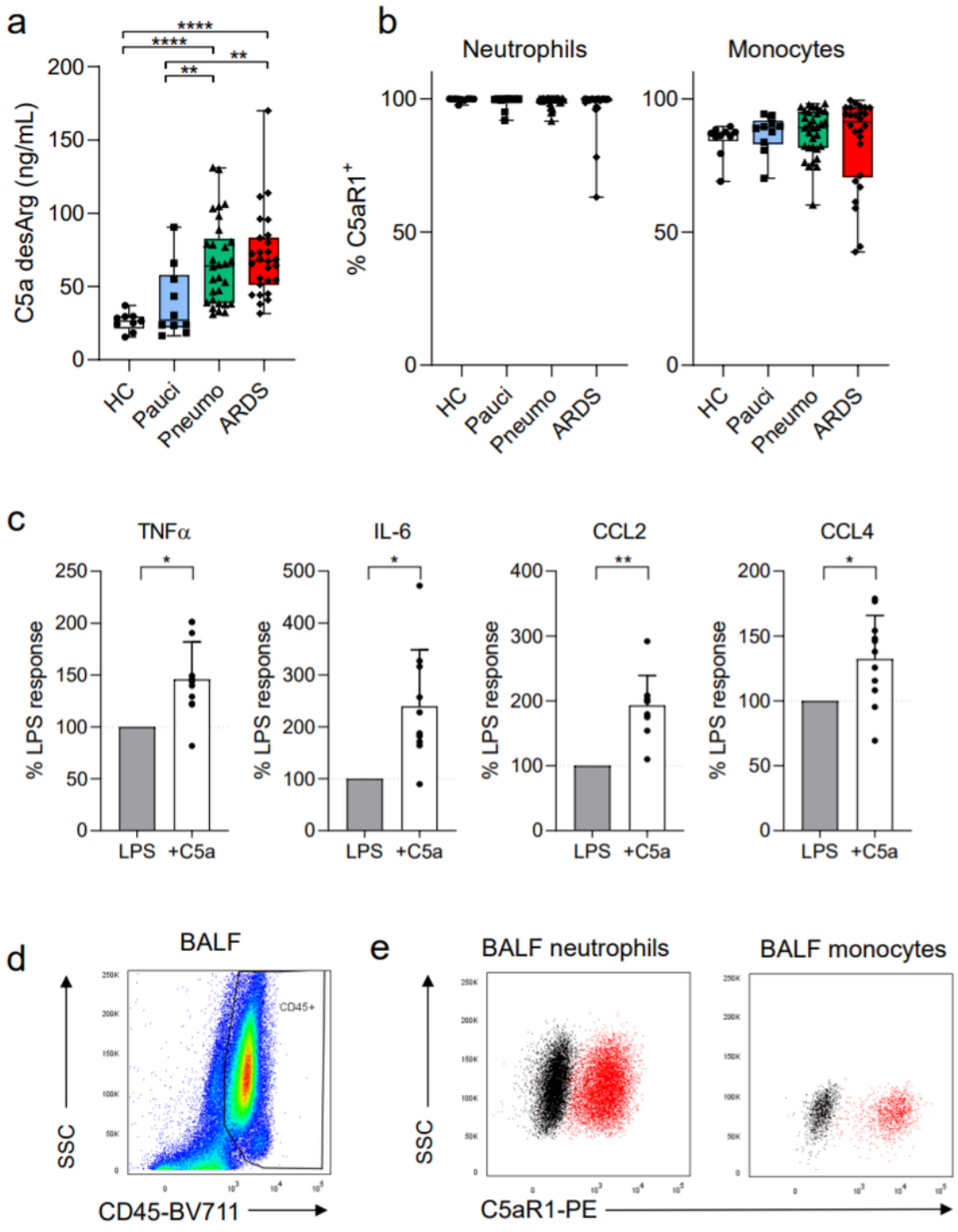

Figure 3

l Up-regulation of the C5a-C5aR1 axis in COVID-19 patients. a, C5a desArg concentration in plasma from healthy donors and COVID-19 patients at T0. Each symbol represents a single donor. b, Percentage of

C5AR1+ neutrophils and monocytes in peripheral blood from healthy donors and COVID-19 patients at T0. Each symbol represents a single donor. a-b, HC (healthy controls, white, n=9), Pauci (paucisymptomatic, blue, n=10), Pneumo (pneumonia, green, n=30 to 32) and ARDS (red, n=26 to 27). c, IL-6, CCL4, CCL2 and TNFa production by monocytes purified from PBMCs from COVID-19 patients activated overnight with LPS (0.5 ng/mL) and C5a (1 µg/mL), when indicated. Data show the percentage response to LPS stimulation alone. Each dot represents the mean value obtained from duplicate or triplicate analysis for a single patient (n=12 patients). d, CD45+ immune cell infiltration in BALF from ARDS patients visualized by FACS. e, C5aR1 expression (red) vs. FMO (black) staining on CD45+CD14-CD15+CD16+ neutrophils and CD45+CD33+HLADR+CD14+ monocytes in BALF from ARDS patients. d-e, The images shown are representative of analyses performed on samples from 3 ARDS patients. The p-values were computed using Wilcoxon tests: *p<0.05; **p<0.01; ***p<0.001;****p<0.0001.

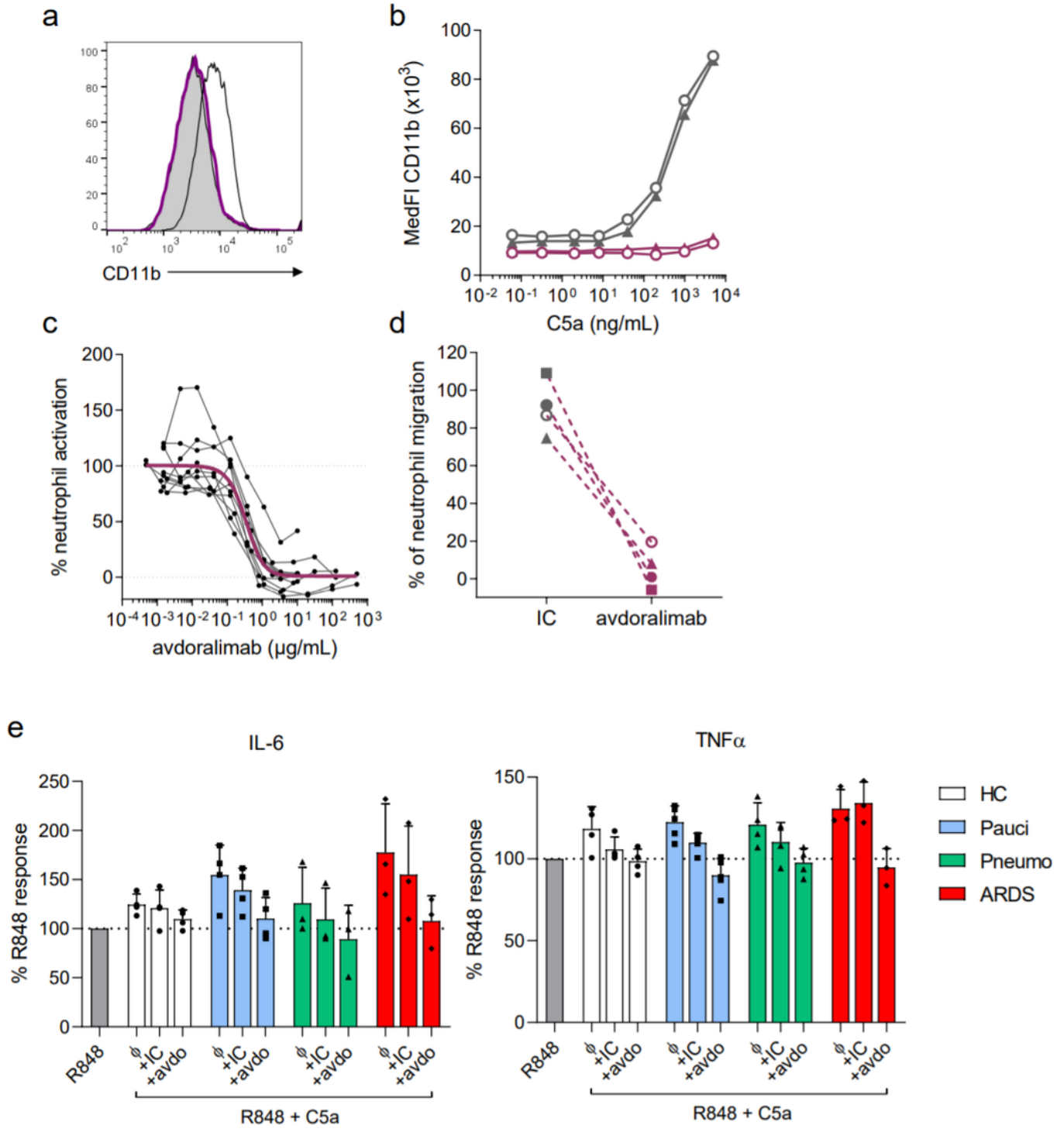

Figure 4

l Avdoralimab, a therapeutic mAb targeting C5aR1, blocks C5a-mediated myeloid cell activation and migration. a, Representative FACS histogram of the inhibition, by avdoralimab, of C5a-mediated CD11b upregulation on whole-blood neutrophils. The grey line corresponds to non-activated neutrophils; the black line corresponds to C5a-activated neutrophils and the purple line corresponds to avdoralimab (30 µg/mL)-treated neutrophils activated by C5a. b, Dose-dependent induction of CD11b in response to C5a

in untreated (gray) or avdoralimab (10 μg/mL)-treated whole-blood neutrophils (purple). The data shown were obtained with cells from two independent donors. c, The percentage of neutrophil activation, monitored by CD11b upregulation, is decreased by increasing doses of avdoralimab. Each gray line represents data from a single donor. The purple line represents a non-linear curve fitted to model the blockade, by avdoralimab, of neutrophil activation by C5a. d, Percentages of neutrophil migration induced by C5a. Neutrophils were treated with 10 μg/mL isotype control (gray) or avdoralimab (purple) before the induction of migration. The image shows neutrophils purified from 4 healthy donors. e, IL-6 and TNF production by monocytes purified from PBMC from HC and COVID-19 patients and activated by overnight incubation with R848 (50 ng/mL) alone or in combination with C5a (1 μg/mL), when indicated. Before activation, monocytes were left untreated (Φ) or subjected to preincubation with 20 μg/mL avdoralimab (avdo) or isotype control (IC), when indicated. The data shown are the percentage increase relative to stimulation with R848 alone. Each dot represents a mean value obtained from duplicate or triplicate analysis for a single donor. HC (healthy controls, white, n=4), Pauci (paucisymptomatic, blue, n=5), Pneumo (pneumonia, green, n=4) and ARDS (red, n=3).

Supplementary Files

This is a list of supplementary files associated with this preprint. Click to download.

- ExtFig1.png
- ExtFig3.png
- 20200406540Asuppfigs.pptx